The Astrophysical Journal, 848:98 (8pp), 2017 October 20 https://doi.org/10.3847/1538-4357/aa8c74

The ^{95}Zr(n, γ)^{96}Zr Cross Section from the Surrogate Ratio Method and Its Effect on s-process Nucleosynthesis

S. Q. Yan (颜胜权)[1], Z. H. Li (李志宏)[1], Y. B. Wang (王友宝)[1], K. Nishio[2], M. Lugaro[3,4], A. I. Karakas[4], H. Makii[2], P. Mohr[5,6], J. Su (俊苏)[1], Y. J. Li (李云居)[1], I. Nishinaka[2], K. Hirose[2], Y. L. Han (韩银录)[1], R. Orlandi[2], Y. P. Shen (谌阳平)[1], B. Guo (冰郭)[1], S. Zeng (晟曾)[1], G. Lian (钢连)[1], Y. S. Chen (陈永寿)[1], and W. P. Liu (柳卫平)[1]

[1] China Institute of Atomic Energy, P.O. Box 275(10), Beijing 102413, P. R. China; panyu@ciae.ac.cn
[2] Japan Atomic Energy Agency, Tokai, Naka, Ibaraki 319-1195, Japan
[3] Konkoly Observatory, Research Centre for Astronomy and Earth Sciences, Hungarian Academy of Sciences, 1121 Budapest, Hungary; maria.lugaro@csfk.mta.hu
[4] Monash Centre for Astrophysics, School of Physics and Astronomy, Monash University, Clayton, VIC 3800, Australia
[5] Institute for Nuclear Research (ATOMKI), H-4001 Debrecen, Hungary
[6] Diakonie-Klinikum, D-74523 Schwäbisch Hall, Germany

Received 2017 May 14; revised 2017 September 10; accepted 2017 September 11; published 2017 October 17

Abstract

The ^{95}Zr(n, γ)^{96}Zr reaction cross section is crucial in the modeling of s-process nucleosynthesis in asymptotic giant branch stars because it controls the operation of the branching point at the unstable ^{95}Zr and the subsequent production of ^{96}Zr. We have carried out the measurement of the ^{94}Zr(^{18}O, ^{16}O) and ^{90}Zr(^{18}O, ^{16}O) reactions and obtained the γ-decay probability ratio of ^{96}Zr* and ^{92}Zr* to determine the ^{95}Zr(n, γ)^{96}Zr reaction cross sections with the surrogate ratio method. Our deduced Maxwellian-averaged cross section of 66 $\pm$ 16 mb at 30 keV is close to the value recommended by Bao et al., but 30% and more than a factor of two larger than the values proposed by Toukan & Käppeler and Lugaro et al., respectively, and routinely used in s-process models. We tested the new rate in stellar models with masses between 2 and 6 $M_{\odot}$ and metallicities of 0.014 and 0.03. The largest changes—up to 80% variations in ^{96}Zr—are seen in models of mass 3–4 $M_{\odot}$, where the ^{22}Ne neutron source is mildly activated. The new rate can still provide a match to data from meteoritic stardust silicon carbide grains, provided that the maximum mass of the parent stars is below 4 $M_{\odot}$, for a metallicity of 0.03.

Key words: nuclear reactions, nucleosynthesis, abundances – stars: AGB and post-AGB

1. Introduction

Elements heavier than iron are produced via neutron captures: the *slow* neutron-capture process (s-process) and the *rapid* neutron-capture process (r-process), except for a minor contribution from the so-called p-process (Burbidge et al. 1957; Seeger et al. 1965; Wallerstein et al. 1997). The r-process is associated with explosive nucleosynthesis in core-collapse supernovae or neutron star mergers. Because of the extremely high neutron densities ($\gg 10^{20}$ cm^{-3}), the timescale for neutron-capture is of the order of milliseconds, and the neutron-capture path involves very neutron-rich nuclei, which decay to their corresponding isobars once the neutron flux is extinguished. The s-process is associated with the thermally pulsating asymptotic giant branch (TP-AGB) phases of low-mass (<8 $M_{\odot}$) stars (Gallino et al. 1988; Meyer 1994; Gallino et al. 1998; Arlandini et al. 1999; Busso et al. 1999; Goriely & Mowlavi 2000; Cristallo et al. 2009; Bisterzo et al. 2011; Lugaro et al. 2012; Karakas & Lattanzio 2014) and the evolutionary hydrostatic phases of more massive (>10 $M_{\odot}$) stars (Käppeler et al. 1989; Raiteri et al. 1991; Travaglio et al. 2004; Pignatari et al. 2010; Frischknecht et al. 2012), which contribute to the main and strong s-component from Sr to Pb/Bi and the weak s-component between Fe and Sr, respectively. The neutron densities for the s-process are of the order of 10^{6}–10^{13} cm^{-3}, the timescale of neutron-capture (order of years) is usually much larger than the average half-lives of β-unstable nuclei, and the reaction path of the s-process thus follows the valley of β stability.

Zirconium is a typical s-process element belonging to the first s-process peak and is mostly produced by the main component in AGB stars. Its isotopic abundances are sensitive to both the neutron exposure and the neutron density, thus they are critical to constraining the s-process in AGB stars (Lugaro et al. 2003). Because of their near-magic neutron configuration, all isotopes of Zr have relatively small (n, γ) cross sections, therefore they have comparably high s-abundances. Zirconium is one of a dozen elements heavier than iron (Kr, Sr, Zr, Mo, Ba, Xe, Nd, Sm, Dy, Eu, W, Pb) whose isotopic abundances can be obtained from the meteoritic stardust grains with high precision (Nicolussi et al. 1997; Gunther et al. 1998; Barzyk et al. 2007; Ávila et al. 2012a, 2012b, 2013). The Zr abundances can also be spectroscopically observed in cool stars (Lambert et al. 1995) and post-AGB stars (Van Winckel 2003; De Smedt et al. 2012).

The most neutron-rich stable Zr isotope, ^{96}Zr, is very sensitive to the neutron density during the s-process because its production depends on the activation of the branching point at ^{95}Zr (with a half-life of 64 days) for neutron densities above roughly 10^{10} cm^{-3}. In low-mass AGB stars, the main neutron source is the ^{13}C(α, n)^{16}O reaction, which produces neutrons with densities lower than 10^{8} cm^{-3}. In this condition, the abundance of ^{96}Zr is depleted by neutron captures and not replenished. On the other hand, during the phase of He shell flashes, the temperature can reach up to 3.5×10^{8} K as the stellar mass increases and the ^{22}Ne neutron source is activated, which results in neutron densities of up to 10^{13} cm^{-3} (Fishlock et al. 2014). Since ^{96}Zr has a low neutron-capture cross section (Tagliente et al. 2011b), once it is produced it tends to accumulate. Thus, the s-abundance of ^{96}Zr can be developed as a tool to probe the neutron density in the stellar interior and be interpreted as an indicator for the efficiency of the ^{22}Ne neutron source and the stellar mass.

With this aim, isotopic abundances obtained from stardust grains and astronomical observations should be compared to the stellar nucleosynthesis calculations. However, while the neutron cross sections of the stable Zr isotopes have been carefully studied (Tagliente et al. 2008a, 2008b, 2010, 2011a, 2011b, 2013), the cross section of the ^{95}Zr(n, γ)^{96}Zr reaction is still extremely uncertain. It is hard to measure the cross section directly due to the difficulty of preparing the target of the short-lived radionuclide ^{95}Zr. Because of the lack of experimental data, the theoretical cross-section estimates for the Maxwellian Averaged Cross-Section (MACS) at $kT = 30$ keV vary from 25 to 140 mb (KADoNiS v0.3[7]). The values estimated by Bao et al. (2000), (79 ± 12 mb at $kT = 30$ keV), Toukan & Käppeler (1990), (50 mb at $kT = 30$ keV), or Lugaro et al. (2014) (28 mb at $kT = 30$ keV) are usually adopted in the stellar models. The recommendation by Bao et al. (2000) of 79 ± 12 mb has been adopted in the KADoNiS v0.3 database (Dillmann et al. 2009), but will be replaced in the next version, KADoNiS v1.0 (I. Dillmann 2016, private communication), by 106 ± 26 mb, which is the average from two recent theoretical evaluations TENDL-2015 (Koning et al. 2015) and ENDF/B-VII.1 (Chadwick et al. 2011). Because of these large discrepancies in the calculation of the MACS of ^{95}Zr(n, γ)^{96}Zr, improved data are of paramount importance.

Recently, the ^{96}Zr(γ, n)^{95}Zr cross section was measured to constrain the γ-ray strength function, and the HFB-QRPA model was used to obtain the ^{95}Zr(n, γ)^{96}Zr cross section (Utsunomiya et al. 2010). Here, we present the first experimental effort to obtain the (n, γ) cross section of ^{95}Zr using the surrogate ratio method (SRM), based on a benchmark experiment already performed to validate the method (Yan et al. 2016).

2. ^{95}Zr(n, γ)^{96}Zr Cross Sections

2.1. Surrogate Ratio Method

The SRM is a variation of the surrogate method (Younes & Britt 2003a, 2003b; Petit et al. 2004; Boyer et al. 2006; Kessedjian et al. 2010). The SRM has been successfully employed in (n, f) cross-section determination for years (Plettner et al. 2005; Burke et al. 2006; Lyles et al. 2007; Nayak et al. 2008; Goldblum et al. 2009; Lesher et al. 2009; Ressler et al. 2011). A comprehensive review can be found in Escher et al. (2012) that includes both the absolute surrogate method and relative ratio method.

Based on the Weisskopf–Ewing limit of the Hauser–Feshbach theory (Weisskopf & Ewing 1940), the γ-decay probability is independent of the spin-parity of the compound nucleus (CN), therefore the cross section of ^{95}Zr(n, γ)^{96}Zr can be expressed as

$$\sigma_{^{95}\mathrm{Zr}(n,\gamma)}(E_n) = \sigma^{\mathrm{CN}}_{n+^{95}\mathrm{Zr}}(E_n) G^{\mathrm{CN}}_{^{96}\mathrm{Zr}^*\rightarrow{}^{96}\mathrm{Zr}+\gamma}(E_n). \quad (1)$$

In the above equation, $\sigma^{\mathrm{CN}}_{n+^{95}\mathrm{Zr}}(E_n)$ denotes the CN-forming cross section and $G^{\mathrm{CN}}_{^{96}\mathrm{Zr}^*\rightarrow{}^{96}\mathrm{Zr}+\gamma}(E_n)$ represents the γ-decay probability of ^{96}Zr*, where E_n is the incident energy of a neutron. Here, ^{96}Zr* is formed via a surrogate reaction, ^{18}O + ^{94}Zr $\rightarrow{}^{16}$O + ^{96}Zr*, and the γ decay of ^{96}Zr* is observed in coincidence with the outgoing particle ^{16}O. The γ-decay probability of ^{96}Zr* can be written as

$$G^{\mathrm{CN}}_{^{96}\mathrm{Zr}^*\rightarrow{}^{96}\mathrm{Zr}+\gamma}(E_{\mathrm{ex}}) = \frac{N_{\gamma(^{96}\mathrm{Zr}^*)}(E_{\mathrm{ex}})}{\epsilon_\gamma N_{^{96}\mathrm{Zr}^*}(E_{\mathrm{ex}})}, \quad (2)$$

where $N_{^{96}\mathrm{Zr}^*}(E_{\mathrm{ex}})$ is the total number of ^{96}Zr* and $N_{\gamma(^{96}\mathrm{Zr}^*)}(E_{\mathrm{ex}})$ is the observed number of ^{96}Zr* that decays finally into the ground state by emitting γ-rays. The E_{ex} symbol denotes the excitation energy of ^{96}Zr* and ϵ_γ is the efficiency of the γ detector.

To derive the ^{95}Zr(n, γ)^{96}Zr reaction cross section using the SRM, a reference reaction with a known cross section is needed. We chose ^{91}Zr(n, γ)^{92}Zr as the reference reaction, then the ratio of the two reaction cross sections is

$$\begin{aligned}\frac{\sigma_{^{95}\mathrm{Zr}(n,\gamma)}(E_n)}{\sigma_{^{91}\mathrm{Zr}(n,\gamma)}(E_n)} &= \frac{\sigma^{\mathrm{CN}}_{n+^{95}\mathrm{Zr}}(E_n) \times G^{\mathrm{CN}}_{^{96}\mathrm{Zr}^*\rightarrow{}^{96}\mathrm{Zr}+\gamma}(E_n)}{\sigma^{\mathrm{CN}}_{n+^{91}\mathrm{Zr}}(E_n) \times G^{\mathrm{CN}}_{^{92}\mathrm{Zr}^*\rightarrow{}^{92}\mathrm{Zr}+\gamma}(E_n)} \\ &\approx \frac{G^{\mathrm{CN}}_{^{96}\mathrm{Zr}^*\rightarrow{}^{96}\mathrm{Zr}+\gamma}(E_n)}{G^{\mathrm{CN}}_{^{92}\mathrm{Zr}^*\rightarrow{}^{92}\mathrm{Zr}+\gamma}(E_n)} \\ &= \frac{\epsilon_{\gamma(^{92}\mathrm{Zr}^*)} N_{\gamma(^{96}\mathrm{Zr}^*)}(E_n)}{\epsilon_{\gamma(^{96}\mathrm{Zr}^*)} N_{\gamma(^{92}\mathrm{Zr}^*)}(E_n)} \times \frac{N_{^{92}\mathrm{Zr}^*}(E_n)}{N_{^{96}\mathrm{Zr}^*}(E_n)}. \end{aligned} \quad (3)$$

The reference reaction is chosen to be similar to the desired reaction so that their CN formation cross sections are almost the same. A theoretical calculation using the UNF code (Zhang 1992, 1993, 2002) shows that the two CN formation cross sections are almost equal within 7% difference. Thus, $\sigma^{\mathrm{CN}}_{n+^{95}\mathrm{Zr}}(E_n)/\sigma^{\mathrm{CN}}_{n+^{91}\mathrm{Zr}}(E_n) \approx 1$ and the (n, γ) cross-section ratio can be simplified to the ratio of γ-decay probabilities.

In the SRM experiment we use ^{94}Zr(^{18}O, ^{16}O)^{96}Zr* and ^{90}Zr(^{18}O, ^{16}O)^{92}Zr* reactions to form the compound nuclei ^{96}Zr* and ^{92}Zr*, respectively. The ratio $N_{^{92}\mathrm{Zr}^*}(E_{\mathrm{ex}})/N_{^{96}\mathrm{Zr}^*}(E_{\mathrm{ex}})$ in Equation (3) can be determined from the CN formation cross section integrated over the detector solid angle $\sigma^{\mathrm{CN}}_{\mathrm{Zr}^*}(E_{\mathrm{ex}})$, the thickness of target ρ, the beam current I, and the efficiency of the particle detector ϵ_p through the relation

$$\begin{aligned}\frac{N_{^{92}\mathrm{Zr}^*}(E_{\mathrm{ex}})}{N_{^{96}\mathrm{Zr}^*}(E_{\mathrm{ex}})} &= \frac{\sigma^{\mathrm{CN}}_{^{90}\mathrm{Zr}(^{18}\mathrm{O},^{16}\mathrm{O})^{92}\mathrm{Zr}^*}(E_{\mathrm{ex}})}{\sigma^{\mathrm{CN}}_{^{94}\mathrm{Zr}(^{18}\mathrm{O},^{16}\mathrm{O})^{96}\mathrm{Zr}^*}(E_{\mathrm{ex}})} \\ &\quad \times \frac{\rho_{(^{90}\mathrm{Zr})} \times I_{^{18}\mathrm{O}(^{90}\mathrm{Zr})} \times \epsilon_{p(^{90}\mathrm{Zr})}}{\rho_{(^{94}\mathrm{Zr})} \times I_{^{18}\mathrm{O}(^{94}\mathrm{Zr})} \times \epsilon_{p(^{94}\mathrm{Zr})}}. \end{aligned} \quad (4)$$

We identified the ejectile nucleus ^{16}O with a silicon telescope to determine the excitation energy of corresponding CN; $\epsilon_{p(^{90}\mathrm{Zr})}$ and $\epsilon_{p(^{94}\mathrm{Zr})}$ can be canceled since the two surrogate reactions are measured in the same experimental setup. The two surrogate reactions are chosen to be similar so that $\sigma^{\mathrm{CN}}_{^{92}\mathrm{Zr}^*}(E_{\mathrm{ex}})/\sigma^{\mathrm{CN}}_{^{96}\mathrm{Zr}^*}(E_{\mathrm{ex}}) \approx 1$, and Equation (3) becomes

$$\begin{aligned}\frac{\sigma_{^{95}\mathrm{Zr}(n,\gamma)}(E_n)}{\sigma_{^{91}\mathrm{Zr}(n,\gamma)}(E_n)} &\approx \frac{N_{\gamma(^{96}\mathrm{Zr}^*)}(E_n)}{N_{\gamma(^{92}\mathrm{Zr}^*)}(E_n)} \\ &\quad \times \frac{\epsilon_{\gamma(^{92}\mathrm{Zr}^*)} \times \rho_{(^{90}\mathrm{Zr})} \times I_{^{18}\mathrm{O}(^{90}\mathrm{Zr})}}{\epsilon_{\gamma(^{96}\mathrm{Zr}^*)} \times \rho_{(^{94}\mathrm{Zr})} \times I_{^{18}\mathrm{O}(^{94}\mathrm{Zr})}} \\ &\approx C_{\mathrm{nor}} \frac{N_{\gamma(^{96}\mathrm{Zr}^*)}(E_n)}{N_{\gamma(^{92}\mathrm{Zr}^*)}(E_n)}. \end{aligned} \quad (5)$$

The normalization factor C_{nor} can be evaluated by correcting the target thickness, the beam current, and the γ-ray efficiency

[7] http://www.kadonis.org

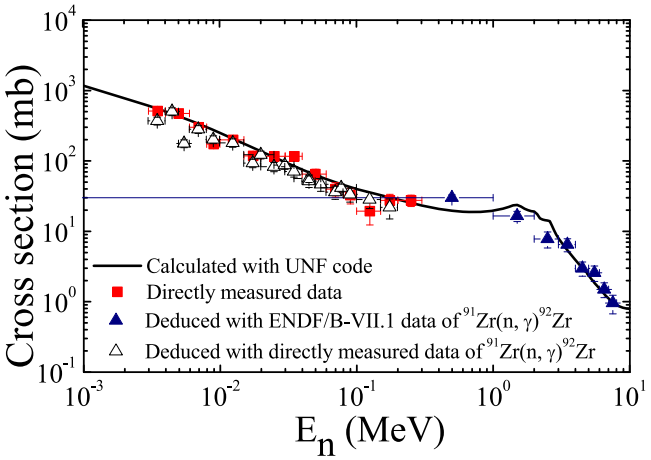

Figure 1. Cross section of ^{93}Zr(n, γ)^{94}Zr. The red squares are directly measured data (Macklin 1985), the open triangles are deduced by the γ-decay probability ratio and ^{91}Zr(n, γ)^{92}Zr cross sections (Musgrove et al. 1977), the blue triangles are deduced by the γ-decay probability ratios and the ^{91}Zr(n, γ)^{92}Zr ENDF/B-VII.1 cross section, and the solid curve is the results calculated by the UNF code.

$\epsilon_{\gamma(^{92}\mathrm{Zr}^*)}$, $\epsilon_{\gamma(^{96}\mathrm{Zr}^*)}$ of the two surrogate reactions. After $N_{\gamma(^{96}\mathrm{Zr}^*)}(E_n)$ and $N_{\gamma(^{92}\mathrm{Zr}^*)}(E_n)$ are obtained experimentally, the cross section of the ^{95}Zr(n, γ)^{96}Zr reaction can be extracted using the known cross section of the reference reaction ^{91}Zr(n, γ)^{92}Zr. Since the total number of CNs $N_{\mathrm{Zr}^*}(E_{\mathrm{ex}})$ is not needed in SRM, uncertainties arising from $N_{\mathrm{Zr}^*}(E_n)$ are eliminated.

2.2. Benchmark Experiment

Before this work, a benchmark experiment (Yan et al. 2016) was carried out to check the validity of SRM in (n, γ) cross-section determinations. In that experiment, the ^{91}Zr(n, γ)^{92}Zr was chosen as the reference reaction and the ^{90}Zr(^{18}O,^{16}O) and ^{92}Zr(^{18}O,^{16}O) reactions were taken as the surrogate reactions to populate the neutron resonance states in ^{92}Zr and ^{94}Zr in a large range of equivalent neutron energies. The relative γ-decay probability ratios of the neutron resonance states in ^{94}Zr and ^{92}Zr were measured, and the cross section of the ^{93}Zr(n, γ)^{94}Zr reaction was derived from the experimentally obtained ratios and the cross sections of the ^{91}Zr(n, γ)^{92}Zr reaction in the equivalent neutron energy range of E_n = 0–8 MeV. The deduced cross sections of the ^{93}Zr(n, γ)^{94}Zr reaction agree with the directly measured ones in the low-energy region, as shown in Figure 1. A UNF theoretical calculation with the code parameters constrained by the deduced data of the ^{93}Zr(n, γ)^{94}Zr reaction at $E_n > 3$ MeV also agrees well with the directly measured cross sections.

2.3. Measurement

The experiment was carried out at the Tandem-accelerator located at the Japan Atomic Energy Agency (JAEA). The details of the experimental setup can be found in Yan et al. (2016). An ^{18}O beam with an energy of 117 MeV bombarded the isotopically enriched zirconium target, which was made in the form of self-supporting metallic foil. The ^{90}Zr target had a thickness of 300 μg/cm^2 and an isotopical enrichment of 99.4%; while the ^{94}Zr target had a thickness of 350 μg/cm^2 and an isotopical enrichment of 96.3%. Downstream of the target, a silicon detector telescope $\Delta E - E$ (Nishio et al. 2015) was

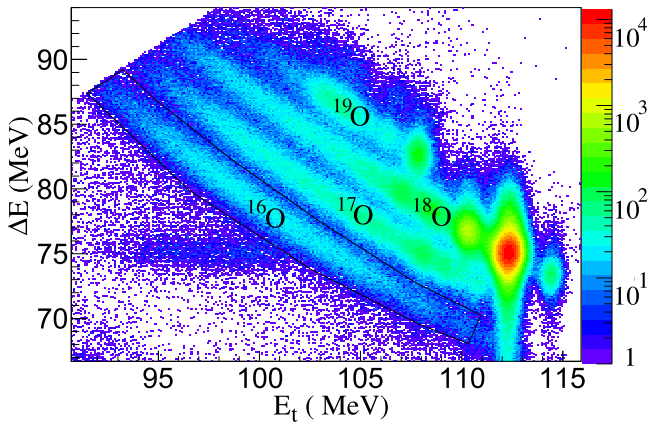

Figure 2. Scatter plot of energy loss vs. total energy of the reaction products from ^{18}O + ^{94}Zr.

used to identify the light ejectile particles, and two $LaBr_3$(Ce) detectors with sizes of 4 inch in diameter and 5 inch in length were used for γ-ray detection (Makii et al. 2015). A faraday cup was installed to collect the ^{18}O beam current for normalization purpose. The ^{18}O beam was kept to about 5 enA, and the size of the beam spot was less than 3 mm in diameter.

The beam time for each Zr target was about two days, and the accumulated number of ^{16}O was roughly 5.8×10^5 and 1.2×10^6 for the ^{94}Zr and ^{90}Zr targets, respectively. The detected γ ray events from ^{96}Zr* and ^{92}Zr* were about 5.9×10^2 and 1.9×10^3, respectively.

2.4. Data Analysis

The recoil ^{16}O was used to reconstruct the excitation energy E_x of ^{92}Zr* or ^{96}Zr* by two-body kinematics, and the γ-rays were extracted in coincidence with the corresponding CNs to obtain the $N_{\gamma(^{96}\mathrm{Zr}^*)}(E_n)$ and $N_{\gamma(^{92}\mathrm{Zr}^*)}(E_n)$ in Equation (5). The two-dimensional scatter plot of energy loss (ΔE) versus total energy (E_t) was used to identify the recoil ^{16}O. E_t is the sum of energy loss in the ΔE detector and the residual energy in the silicon ring detector. As an example, the $\Delta E - E_t$ scatter plot corresponding to the second inner ring of the annular E detector is shown in Figure 2, with a cut to select ^{16}O events from the (^{18}O,^{16}O) two-neutron transfer reaction. The energy resolution for ^{16}O was about 1 MeV in full width at half maximum (FWHM), which was mainly due to the noise of silicon detectors and the kinematic uncertainty originated from the 1.2 degree resolution of each ring.

Since ^{92}Zr and ^{96}Zr are both even–even nuclei, the de-excitation of their high-lying resonance states is expected to proceed overwhelmingly through the first 2^+ state to the 0^+ ground state doorway transition. The energy of the transition is 1750 keV for ^{96}Zr*, and 934 keV for ^{92}Zr*. First, we deduced the net areas of these two γ lines in a bin width of E_n = 1000 keV. The net areas were then normalized to the integrated ^{18}O beam current, the target thickness, and the absolute detection efficiency of the $LaBr_3$ detectors, for each of the ^{94}Zr(^{18}O, ^{16}Oγ)^{96}Zr and ^{90}Zr(^{18}O, ^{16}Oγ)^{92}Zr runs. The minor difference of solid angle due to the tiny difference of reaction kinematics for the ^{94}Zr and ^{90}Zr target runs was also taken into account. The absolute branching ratios of the 1750 and 934 keV γ lines in ^{96}Zr and ^{92}Zr were taken as 80.0% and 91.7%, respectively, from the in-beam ^{96}Zr(p, p$'\gamma$) study

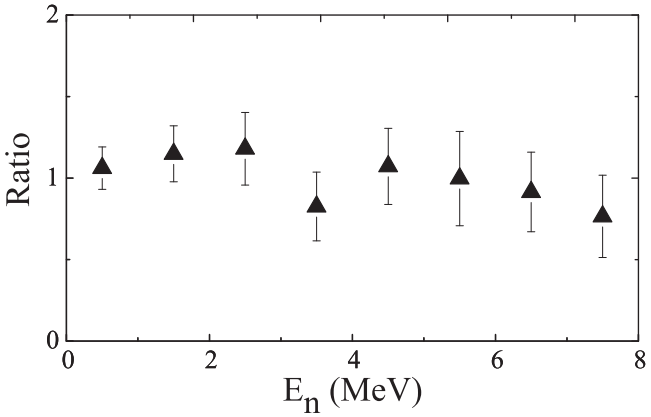

Figure 3. The γ-decay probability ratio of the compound nuclei ^{96}Zr* and ^{92}Zr*.

(Molnár et al. 1989) and the prompt γ-ray spectroscopy study (Nakamura et al. 2007) of the ^{91}Zr(n, γ)^{92}Zr reaction. After the corrections were made, the ratio of the γ decay probabilities $N_{^{96}\mathrm{Zr}^*\gamma}(E_n)/N_{^{92}\mathrm{Zr}^*\gamma}(E_n)$ was obtained, as shown in Figure 3. The energy resolution in the equivalent neutron energy E_n is about 1 MeV, and altogether eight ratios were deduced within E_n = 0–8 MeV.

2.5. Experimental Cross Sections

For nuclear astrophysics and other applications focusing on (n, γ) reactions, it is important to deduce the (n, γ) cross sections for $E_n < 1$ MeV. The excitation functions of ^{91}Zr(n, γ)^{92}Zr and ^{95}Zr(n, γ)^{96}Zr calculated by Hauser–Feshbach theory have a similar behavior at $E_n < 1$ MeV. The difference between the two (n, γ) cross sections can be approximated by a constant in this energy range; the ^{95}Zr(n, γ)^{96}Zr cross sections can be determined by multiplying the average ratio of 1.06 ± 0.21 at $E_n < 1$ MeV to the directly measured ^{91}Zr(n, γ)^{92}Zr cross sections (Musgrove et al. 1977). The uncertainty of the deduced ^{95}Zr(n, γ)^{96}Zr cross section includes the experimental uncertainty and an additional systematic uncertainty of 10%–15%, which is estimated by the UNF/TALYS (Koning et al. 2016) code by a variation of the parameters of the calculation within a reasonable range. A further essential constraint of the parameter space was obtained from the analysis of the ^{96}Zr(γ, n)^{95}Zr data (Utsunomiya et al. 2010) (see next Section 2.6). The deduced cross sections are shown in Figure 4 as open triangles.

According to Chiba & Iwamoto (2010), the γ-decay probability ratio is relatively insensitive to the spin-parity distribution of CNs at neutron energies $E_n > 3$ MeV. The cross sections in high-energy regions could be used to constrain the parameters of the theoretical calculation. Since there are no experimental data at neutron energies larger than 3 MeV, we used the ENDF/B-VII.1 cross section of the ^{91}Zr(n, γ)^{92}Zr reaction. The ^{95}Zr(n, γ)^{96}Zr reaction cross section was then deduced by the experimental ratio multiplied by the averaged value of the ENDF/B-VII.1 cross section for the ^{91}Zr(n, γ)^{92}Zr reaction. The deduced ^{95}Zr(n, γ)^{96}Zr cross sections are shown in Figure 4 as blue triangles, the width of each energy bin is 1 MeV.

In the determination of (n, γ) cross sections with the SRM, the γ-decay probabilities are assumed to be independent from the spin-parities of CNs in the Weisskopf–Ewing limit of the

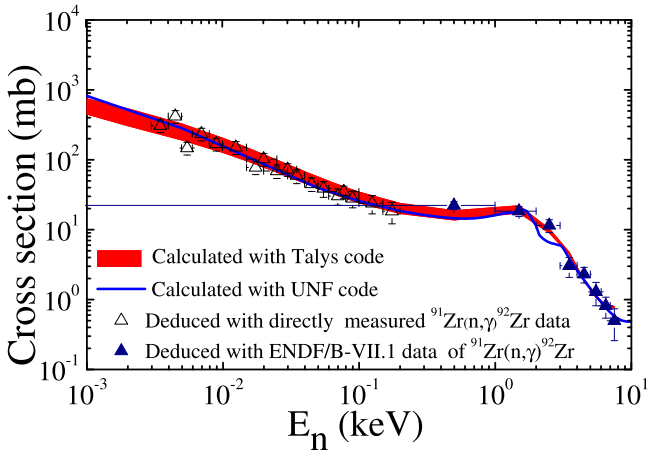

Figure 4. Cross section of ^{95}Zr(n, γ)^{96}Zr. The open triangles are deduced by multiplying our γ-decay probability ratio with the directly measured ^{91}Zr(n, γ)^{92}Zr cross section, and the blue triangles are deduced by multiplying our γ-decay probability ratios with the ENDF data for the ^{91}Zr(n, γ)^{92}Zr cross section.

Hauser–Feshbach theory. However, theoretical study (Chiba & Iwamoto 2010) shows that the γ-decay probability ratio is sensitive to the spin-parity distribution of the CN at low incident neutron energies and it is difficult to determine the (n, γ) cross sections with SRM because the surrogate reactions bring much more angular momentum to the CN compared to low-energy neutrons. Similar to the present work, ^{91}Zr(n, γ)^{92}Zr and ^{93}Zr(n, γ)^{94}Zr were chosen to check the SRM with (^{18}O, ^{16}O) two-neutron transfer reactions in the benchmark experiment described in Section 2.2 (Yan et al. 2016). The ^{93}Zr(n, γ)^{94}Zr reaction cross section deduced by the SRM agrees well with the directly measured ones at $E_n < 1$ MeV, which implies that the sensitivity of the γ-decay probability ratio to the CN spin-parity distribution is partially reduced in SRM at low energies. Furthermore, the theoretical prediction of the ^{93}Zr(n, γ)^{94}Zr reaction agrees with the directly measured value and with the SRM-determined cross sections, and the agreement between theoretical calculations and SRM-determined cross sections of ^{95}Zr(n, γ)^{96}Zr is supportive of our determination.

Finally, in Equation (4), the CN formation cross sections integrated over the detector solid angle ($\sigma^{\mathrm{CN}}_{\mathrm{Zr}^*}(E_{\mathrm{ex}})$) of the two surrogate reactions, ^{94}Zr(^{18}O, ^{16}O)^{96}Zr* and ^{90}Zr(^{18}O, ^{16}O)^{92}Zr*, are supposed to be the same in the formula. In the measurement we verified that the counts of CN ^{96}Zr* and ^{92}Zr*, deduced by the outgoing particle ^{16}O, are almost the same within 9% at $E_n < 8$ MeV, after the corrections of beam current and target thickness.

2.6. Theoretical Excitation Function

The calculation of the astrophysical reaction rate in the next section requires an excitation function of the ^{95}Zr(n, γ)^{96}Zr cross section over a sufficient energy range. In the first stage of the analysis we calculated this excitation function using the statistical model code UNF, and good agreement with the experimental results was found (see Figure 4). These UNF calculations were later extended using the code TALYS for an estimate of the uncertainties. For this purpose the complete parameter space of TALYS was investigated and includes variations of the gamma-ray strength function, the level density, and the nucleon optical model potential. Because of

its negligible influence, the alpha optical model potential was taken from the new TALYS-V1.8 default in the present work. For details of the investigation of the TALYS parameter space, see a similar study on α-induced cross sections on ^{64}Zn (Mohr et al. 2017).

For each combination of TALYS parameters χ^2 values were calculated for the indirect ^{95}Zr(n, γ)^{96}Zr data of the present work and for the data of the reverse ^{96}Zr(γ, n)^{95}Zr reaction by Utsunomiya et al. (2010). These data for the reverse reaction were measured with high precision using monochromatic photons from Laser-Compton scattering. Later average cross sections (Crasta et al. 2014; Naik et al. 2014) from bremsstrahlung are in rough agreement with the monochromatic photon data; because of their larger uncertainties, the bremsstrahlung data were not included in the present χ^2-based adjustment of the TALYS parameters.

For the best fit, an overall $\chi^2/F \approx 3$ was obtained which corresponds to an average deviation factor of 1.2 between the experimental data and the theoretical excitation functions. For the (n, γ) data $\chi^2/F \approx 1.3$ and a similar average deviation of about 1.3 is found; because of the larger uncertainty of the (n, γ) data, χ^2/F is smaller for a similar deviation. The (γ, n) data are described with $\chi^2/F \approx 3.5$ and a small average deviation of 1.1 only. The χ^2/F in the full parameter space of TALYS vary between its minimum value of 3 up to about 300, corresponding to a poor description of the data with an average deviation of a factor of three.

For an estimate of the uncertainty of the ^{95}Zr(n, γ)^{96}Zr cross section, all combinations of TALYS parameters were selected which describe the (n, γ) and (γ, n) data with a reasonable $\chi^2/F \leqslant (\chi^2/F)_{\min} + 1$; for a discussion of this choice, see Mohr et al. (2017). It is found that this choice essentially selects the gamma-ray strength function, whereas the sensitivity of the calculated cross sections to the chosen level density and the chosen nucleon optical model potential remain minor. All reasonable χ^2/F are obtained from the simple Brink-Axel Lorentzian gamma-ray strength function (Brink 1957; Axel 1962; Koning et al. 2016), although recent work has shown that there are additional contributions to the gamma-ray strength function that may affect neutron-capture cross sections that are also close to magic numbers (e.g., Crespo Campo et al. 2016).

The results from all TALYS calculations with reasonable χ^2 are shown in Figure 4 as an error band in comparison with the data extracted by SRM for the ^{95}Zr(n, γ)^{96}Zr reaction. Because the TALYS parameters were adjusted to the experimental data, the excellent agreement is not surprising. Interestingly, the median results of the TALYS calculations and the UNF calculation are very close within a few percent. Thus, the first UNF calculation was used for the calculation of the MACS in the following section. The uncertainty of the MACS of about 25% is estimated from the experimental uncertainty of the SRM data. A similar estimate for the uncertainty is obtained from the study of the TALYS parameter space.

Finally, in Figure 5 we compare the calculated ^{96}Zr(γ, n)^{95}Zr excitation function to the experimental results of Utsunomiya et al. (2010). There is good agreement over the full energy range. It is not surprising that all TALYS calculations with reasonable χ^2 are practically identical because the same gamma-ray strength function is used, and the ^{96}Zr(γ, n)^{95}Zr cross section is practically only sensitive to the gamma-ray strength function but insensitive to the other ingredients of the statistical model.

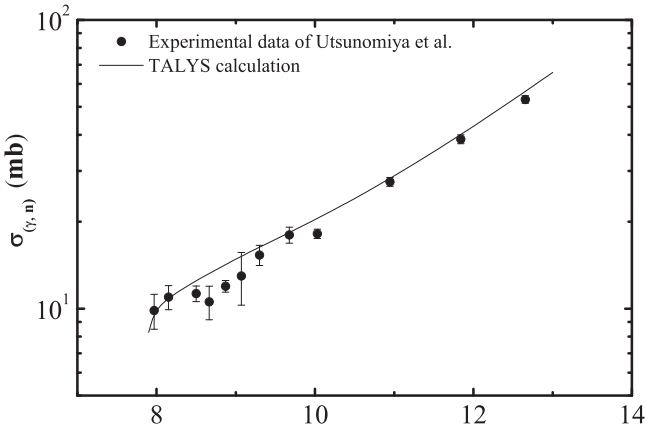

Figure 5. Cross section of ^{96}Zr(γ, n)^{95}Zr. The experimental data of Utsunomiya et al. (2010) are well described by the TALYS calculations of the present work. Note that for this presentation the average of the two analysis methods in Utsunomiya et al. (2010) is shown.

Table 1
Our Derived MACS for ^{95}Zr(n, γ)^{96}Zr in mb

κT (keV)	Tagliente	This Work	Bao
5	255	251 ± 46	296
10	107	153 ± 31	185
15	66	113 ± 24	136
20	46	90 ± 20	109
25	35	76 ± 18	91
30	28	66 ± 16	79 ± 12
40	21	53 ± 14	63
50	16	45 ± 12	54
60	15	40 ± 11	47
80	12	33 ± 10	39
100	11	29 ± 9	34

Note. Also shown for comparison are the MACS by Bao et al. (2000), labeled as Bao, which is based on a semi-empirical analysis of the neighboring nuclei and the MACS from Lugaro et al. (2014; labeled as Tagliente), based on the comparison of the trends shown by the odd-numbered and even-numbered nuclei in the region as done by Toukan & Käppeler (1990), but on the basis of updated neutron-capture cross sections Tagliente et al. (2008a, 2008b, 2010, 2011a, 2011b, 2013).

2.7. Reaction Rate

From the deduced cross sections of ^{95}Zr(n, γ)^{96}Zr reaction, we derived the Maxwellian-Averaged Cross Sections (MACS) shown in Table 1. The MACS of this work is 66 ± 16 mb at $kT = 30$ keV. This value is in-between the Bao et al. (2000) and Toukan & Käppeler (1990) values, but much larger than Lugaro et al.'s (2014) values and smaller than the values of JENDL-3.2 and significantly smaller than those of ENDF/B-VII.1 and TENDL.

For completeness, we point out that the MACS and the astrophysical reaction rate are almost entirely defined by the laboratory cross section of the ^{95}Zr(n, γ)^{96}Zr reaction because the first excited state in ^{95}Zr at an excitation energy of 954 keV has a negligible thermal population at s-process temperatures. Thus, the stellar enhancement factor remains very close to unity, and the ground state contribution to the astrophysical rate is almost 100% (Rauscher et al. 2011). A suggested candidate for a very low-lying excited state in ^{95}Zr at 23 keV has been definitely excluded by a high-resolution ^{94}Zr(d, p)^{95}Zr experiment (Sonnabend et al. 2003).

Table 2
Variations in the Final Abundance of ^{96}Zr (in Units of 10^{-11}) in Selected Stellar AGB Models for Different ^{95}Zr(n, γ)^{96}Zr Values

Mass	Metallicity	Tagliente	This Work	Bao
2 $M_\odot$	0.014	0.95	1.18 (+25%)	1.28 (+35%)
3 $M_\odot$	0.014	3.57	6.39 (+79%)	7.37 (+106%)
6 $M_\odot$	0.014	1.09	1.24 (+14%)	N/A[a]
3 $M_\odot$	0.03	1.97	2.56 (+30%)	2.79 (+42%)
3.5 $M_\odot$	0.03	2.61	3.80 (+46%)	4.25 (+63%)
4 $M_\odot$	0.03	5.44	8.84 (+63%)	9.93 (+83%)

Note. The percent variations with respect to the MACS of Tagliente are reported in parentheses.
[a] This model was not run for time issues, as it takes almost two months. However, we expect a result close to that obtained with the rate from this work.

The corresponding reaction rate as a function of temperature T_9 (in unit of 10^9 K) is fitted with the expression used in the astrophysical reaction rate library REACLIB:

$$N_A\langle\sigma v\rangle = \exp(17.9065 + 0.0025T_9^{-1} - 0.6686T_9^{-1/3} - 2.5117T_9^{1/3} + 1.5193T_9 - 0.3671T_9^{5/3} - 0.4058\ln T_9). \quad (6)$$

The fitting errors are less than 2% in the range from $T_9 = 0.01$ to $T_9 = 2$.

3. Astrophysical Implications

As mentioned in the introduction, during the *s*-process in AGB stars the activation of the branching point at ^{95}Zr controls the abundance of ^{96}Zr. The branching factor, i.e., the probability that ^{95}Zr captures a neutron instead of β-decay, strongly depends on the maximum neutron density achieved in the star. This is controlled mostly by the efficiency of the ^{22}Ne(α, n)^{25}Mg neutron source, which increases with increasing stellar mass and decreasing metallicity. It follows that the production of ^{96}Zr in AGB stars and the impact of the revised value of the neutron-capture cross section of ^{95}Zr depend on the stellar mass and metallicity considered. To illustrate this, in Table 2 we show the effect of the different neutron-capture cross sections of ^{95}Zr on the final abundance of ^{96}Zr for models of different masses (from 2 to 6 $M_\odot$) and two different metallicities, solar (0.014) and roughly twice solar (0.03). A detailed description of the models can be found in Karakas & Lugaro (2016). We run models using the ^{95}Zr(n, γ)^{96}Zr values listed in Table 1.

In AGB stars of masses below roughly 3 $M_\odot$, the main neutron source is the ^{13}C(α, n)^{16}O reaction, which is activated at low temperatures, ~8 keV, and produces low neutron densities, of the order of 10^7 cm^{-3} (Straniero et al. 1997). For neutron densities below 10^9 cm^{-3}, the probability of producing ^{96}Zr is of the order of a few percent or less. It follows that in this mass range, low abundances of ^{96}Zr are produced and the effect of changing the neutron-capture cross section of ^{95}Zr is relatively small, less than ~30%. As the stellar mass increases, higher temperatures are reached and the ^{22}Ne(α, n)^{25}Mg reaction source is activated. This neutron source produces neutron densities of up to 10^{13} cm^{-3} in stars of masses around 6 $M_\odot$ (van Raai et al. 2012). For neutron densities above 10^{11} cm^{-3}, the branching factor at ^{95}Zr is roughly equal to unity, which means that the main path of neutron captures proceeds through ^{96}Zr, instead of ^{95}Mo. In this case, the exact value of the neutron-capture cross section of ^{95}Zr does not play a major role in the production of ^{96}Zr. Rather, it is the value of the neutron-capture cross section of ^{96}Zr itself that counts more, as the abundance of this isotope reaches its equilibrium value. It follows that also in this case the effect on the abundance of ^{96}Zr of changing the neutron-capture cross section of ^{95}Zr is small, 14% for the 6 $M_\odot$ model. The most interesting cases are the intermediate neutron densities values around 10^{10} cm^{-3} that can be reached in AGB stars of masses between 3 and 5 $M_\odot$. For such values of the neutron density the branching factor is roughly 0.5, i.e., there is a 50% probability that ^{95}Zr will decay into ^{95}Mo, and 50% that it will capture a neutron and produce ^{96}Zr. In this regime the effect of changing the neutron-capture cross section of ^{95}Zr has a significant impact, reaching differences of up to a factor of two (Table 2).

In terms of the solar system abundance of ^{96}Zr, Travaglio et al. (2004) derived a contribution of roughly 40% from low-mass AGB stars and roughly 40% from massive AGB stars, using the neutron-capture cross section for ^{95}Zr from Toukan & Käppeler (1990). This is 50 mb at 30 KeV, comparable to the value presented here of 66 ± 16 mb. As illustrated above, the contribution from massive AGB stars does not change when changing the rate; however, for typical low-mass (3–4 $M_\odot$) AGB models, the contribution to the abundance of ^{96}Zr in the solar system would decrease by a factor of up to 80% when using the lower (Tagliente) value of the rate from Lugaro et al. (2014).

Detailed constraints on the operation of the branching point at ^{95}Zr can be derived from the Zr isotopic ratios measured with high precision via mass spectrometry in meteoritic stardust silicon carbide (SiC) grains. These grains originated in C-rich AGB stars (i.e., with masses between roughly 1.5 and 4 $M_\odot$) of metallicity around solar and show the clear signature of the *s*-process. However, to fully extract information from them on processes such as dust formation, galactic chemical evolution, and the composition of the dust inventory present in the presolar nebula, we need to accurately determine the masses and metallicities of their parent stars. This can be done using detailed stellar nucleosynthesis models, where nuclear inputs such as the neutron-capture cross section of ^{95}Zr play a major role. Lugaro et al. (2017) analyzed in detail the comparison between the SiC data and model for AGB stars of solar and twice-solar metallicity. They concluded that AGB stars of metallicity twice-solar are good candidates for the origin of the grains, also based on the fact that the ^{22}Ne neutron source reaction in these stars is activated in such a way that the trend of the ^{96}Zr/^{94}Zr isotopic ratios can be well matched. This conclusion obviously depends on the choice of the ^{95}Zr(n, γ)^{96}Zr rate.

In Figure 6, we show the same selection of models from Karakas & Lugaro (2016) presented in Table 2 and in comparison to the SiC grain data.

Because the value of the rate presented in this work is the same as the value from Bao, within the error bar, but is significantly higher than the value from Tagliente, it results in $\delta(^{96}\mathrm{Zr}/^{94}\mathrm{Zr})$ values ($\delta(^{96}\mathrm{Zr}/^{94}\mathrm{Zr}) = [(^{96}\mathrm{Zr}/^{94}\mathrm{Zr})_{\mathrm{grain}}/(^{96}\mathrm{Zr}/^{94}\mathrm{Zr})_\odot - 1] \times 10^3$) up to 400 permil higher than those computed with the rate from Tagliente. With the new rate the data can still be covered well, considering the uncertainties in the neutron-capture cross section of ^{92}Zr of 10% at 2σ (Tagliente et al. 2010), which would result in variation of ±100 in the $\delta(^{92}\mathrm{Zr}/^{94}\mathrm{Zr})$ values. Interestingly, using the new rate, the range of stellar mass that covers the data

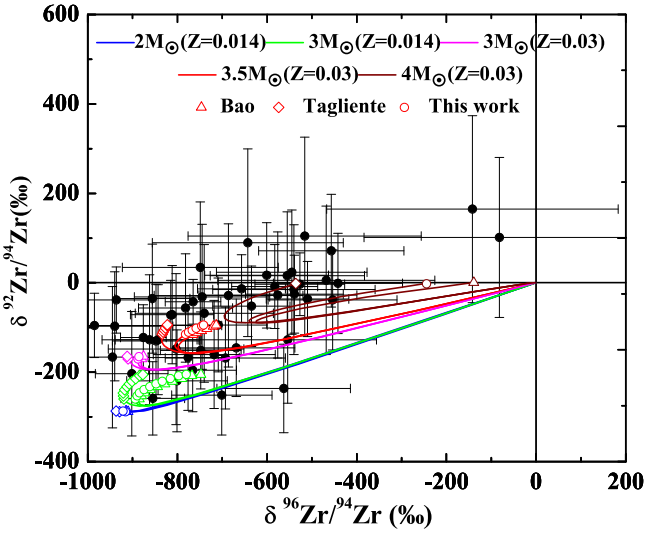

Figure 6. SiC grain data (black circles with 2σ error bars; for references see Liu et al. 2014) are compared to the surface evolution of AGB stellar models for different masses and metallicities from Karakas & Lugaro (2016), using the standard choice of the parameter that controls the formation of the ^{13}C neutron source ($M_{\rm PMZ}$, see that paper for more details). For the comparison, δ-values are used, which represent the permil variations with respect to the solar system ratio, corresponding to the initial value used for the calculations. The straight dashed lines represent the solar composition, with $\delta = 0$ by definition. Each colored line represents the evolution of an AGB star of different initial mass and metallicity, as indicated by the labels. Open symbols on the lines represent the phases when the envelope reaches C/O > 1, the necessary condition for the formation of SiC, with each symbol corresponding to a different ^{95}Zr(n, γ)^{96}Zr rate, as indicated.

would have a maximum below 4 $M_{\odot}$, although this conclusion also depends on the uncertain rate of the ^{22}Ne(α, n)^{25}Mg reaction (Massimi et al. 2017) and the adopted stellar model, as AGB models computed with different codes may vary somewhat in the temperature value that controls the activation of the ^{22}Ne reaction.

4. Summary and Conclusion

In summary, we have determined the ^{95}Zr(n, γ)^{96}Zr reaction cross section using the surrogate ratio method for the first time, and deduced a rate higher than that usually included in models of the *s*-process in AGB stars. The new rate was tested in the stellar models with stellar masses of 2–6 $M_{\odot}$ and metallicities of 0.014 and 0.03. We have seen that the largest effects when changing the rate are seen in models of masses around 3–4 $M_{\odot}$, where the ^{22}Ne(α, n)^{25}Mg neutron source is mildly activated. We also concluded that using the new rate, the masses of the parent stars of meteoritic stardust SiC grains should be somewhat lower than 4 $M_{\odot}$.

This demonstrates the potential of this method to derive better data for neutron-capture cross sections of unstable nuclei relevant to branching points on the *s*-process path. The method could be extended to other nuclei such as ^{85}Kr, ^{107}Pd, and ^{181}Hf, with important implications for model predictions, an impact on the interpretation of observational constraints from spectroscopic to meteoritic data, and the origin of specific isotopes such as ^{96}Zr in the solar system.

We thank the JAEA Tandem-accelerator facility staff for their help in the experiment and the anonymous referee for the constructive suggestions. This work was supported by the National key Research and Development Program of China under grant No. 2016YFA0400502, the National Natural Science Foundation of China under grants No. 11375269, No. 11490560, No. 11321064, the National Basic Research 973 Program of China under grant No. 2013CB834406, and the Hungarian Scientific Research Fund OTKA (K108459 and K120666). M.L. is a Momentum (Lendület-2014 Programme) project leader of the Hungarian Academy of Sciences.This research was undertaken with the assistance of resources from the National Computational Infrastructure (NCI), which is supported by the Australian Government.

Software: UNF (Zhang 1992, 1993, 2002), TALYS (Koning et al. 2016).

ORCID iDs

S. Q. Yan (颜胜权) https://orcid.org/0000-0002-0644-5612
M. Lugaro https://orcid.org/0000-0002-6972-3958
A. I. Karakas https://orcid.org/0000-0002-3625-6951

References

Arlandini, C., Käppeler, F., Wisshak, K., et al. 1999, ApJ, 525, 886
Ávila, J. N., Ireland, T. R., Lugaro, M., et al. 2012a, Lunar Planet. Sci., Vol. 43 (League City, TX: LPI), 2709
Ávila, J. N., Ireland, T. R., Lugaro, M., et al. 2013, ApJL, 768, L18
Ávila, J. N., Lugaro, M., Ireland, T. R., et al. 2012b, ApJ, 744, 49
Axel, P. 1962, PhRv, 126, 671
Bao, Z. Y., Beer, H., Käppeler, F., Voss, F., & Wisshak, K. 2000, ADNDT, 76, 70
Barzyk, J. G., Savina, M. R., Davis, A. M., et al. 2007, M&PS, 42, 1103
Bisterzo, S., Gallino, R., Straniero, O., Cristallo, S., & Käppeler, F. 2011, MNRAS, 418, 284
Boyer, S., Dassié, D., Wilson, J. N., et al. 2006, NuPhA, 775, 175
Brink, D. M. 1957, NuPh, 4, 215
Burbidge, E. M., Burbidge, G. R., Fowler, W. A., & Hoyle, F. 1957, RvMP, 29, 547
Burke, J. T., Bernstein, L. A., Escher, J., et al. 2006, PhRvC, 73, 054604
Busso, M., Gallino, R., & Wasserburg, G. J. 1999, ARA&A, 37, 239
Chadwick, M. B., Herman, M., Obložinský, M., et al. 2011, Nucl. Data Sheets, 112, 2887
Chiba, S., & Iwamoto, O. 2010, PhRvC, 81, 044604
Crasta, R., Naik, H., Suryanarayana, S. V., et al. 2014, Radiochim. Acta., 102, 221
Crespo Campo, L., Bello Garrote, F. L., Eriksen, T. K., et al. 2016, PhRvC, 94, 044321
Cristallo, S., Straniero, O., Gallino, R., et al. 2009, ApJ, 696, 797
De Smedt, K., Van Winckel, H., Karakas, A. I., et al. 2012, A&A, 541, A67
Dillmann, I., Plag, R., Käppeler, F., & Rauscher, T. 2009, in Proc. Scientific Workshop on Neutron Measurements, Theory and Applications, ed. F.-J. Hambsch, 55 http://publications.jrc.ec.europa.eu/repository/handle/JRC56548
Escher, J. E., Burke, J. T., Dietrich, F. S., et al. 2012, RvMP, 84, 353
Fishlock, C. K., Karakas, A. I., Lugaro, M., & Yong, D. 2014, ApJ, 797, 44
Frischknecht, U., Hirschi, R., & Thielemann, F.-K. 2012, A&A, 538, L2
Gallino, R., Arlandini, C., Busso, M., et al. 1998, ApJ, 497, 388
Gallino, R., Busso, M., Picchio, G., Raiteri, C. M., & Renzini, A. 1988, ApJ, 334, 45
Goldblum, B. L., Stroberg, S. R., Allmond, J. M., et al. 2009, PhRvC, 80, 044610
Goriely, S., & Mowlavi, N. 2000, A&A, 362, 599
Gunther, K. N., Michael, J. P., Roy, S. L., et al. 1998, ApJ, 504, 492
Käppeler, F., Beer, H., & Wisshak, K. 1989, RPPh, 52, 945
Karakas, A. I., & Lattanzio, J. C. 2014, PASA, 31, 30
Karakas, A. I., & Lugaro, M. 2016, ApJ, 825, 26
Kessedjian, G., Jurado, B., Aiche, M., et al. 2010, PhLB, 692, 297
Koning, A. J., Hilaire, S., & Goriely, S. 2016, Computer code TALYS, Version 1.8, http://www.talys.eu
Koning, A. J., Rochman, D., Kopecky, J., et al. Evaluation TENDL-2015, https://tendl.web.psi.ch/tendl_2015/tendl2015.html
Lambert, D. L., Smith, V. V., Busso, M., Gallino, R., & Straniero, O. 1995, ApJ, 450, 302
Lesher, S. R., Burkeet, J. T., Bernstein, L. A., et al. 2009, PhRvC, 79, 044609
Liu, N., Gallino, R., Bisterzo, S., et al. 2014, ApJ, 788, 163
Lugaro, M., Davis, A. M., Gallino, R., et al. 2003, ApJ, 593, 486

Lugaro, M., Karakas, A. I., Pető, M., & Plachy, E. 2017, GeCoA, in press
Lugaro, M., Karakas, A. I., Stancliffe, R. J., & Rijs, C. 2012, ApJ, 747, 2
Lugaro, M., Tagliente, G., Karakas, A. I., et al. 2014, ApJ, 780, 95
Lugaro, M., Ugalde, C., Karakas, A. I., et al. 2004, ApJ, 615, 934
Lyles, B. F., Bernstein, L. A., Burke, J. T., et al. 2007, PhRvC, 76, 014606
Macklin, R. L. 1985, Ap&SS, 115, 71
Makii, H., Ota, S., Ishii, T., et al. 2015, NIMA, 83, 797
Massimi, C., Altstadt, S., Andrzejewski, J., et al. 2017, PhLB, 768, 1
Meyer, B. 1994, ARA&A, 32, 153
Mohr, P., Gyürky, Gy., & Fülöp, Zs. 2017, PhRvC, 95, 015807
Molnár, G., Belgya, T., Fazekkas, B., et al. 1989, NuPhA, 500, 43
Musgrove, A. R. d. L., Boldeman, J. W., Allen, B. J., Harvey, J. A., & Macklin, R. L. 1977, AuJPh, 30, 391
Naik, H., Kim, G. N., Schwengner, R., et al. 2014, EPJA, 50, 83
Nakamura, S., Harada, H., Raman, S., & Koehler, P. E. 2007, Journal of Nuclear Science and Technology, 44, 21
Nayak, B. K., Saxena, A., Biswas, D. C., et al. 2008, PhRvC, 78, 061602(R)
Nicolussi, G. K., Davis, A. M., Pellin, M. J., et al. 1997, Sci, 277, 1281
Nishio, K., Hirose, K., Léguillon, R., et al. 2015, PhPro, 64, 140
Petit, M., Aicheet, M., Barreau, G., et al. 2004, NuPhA, 735, 345
Pignatari, M., Gallino, R., Heil, M., et al. 2010, ApJ, 710, 1557
Plettner, C., Ai, H., Beausang, C. W., et al. 2005, PhRvC, 71, 051602(R)
Raiteri, C. M., Busso, M., Gallino, R., & Picchio, G. 1991, ApJ, 371, 665
Rauscher, T., Mohr, P., Dillmann, I., & Plag, R. 2011, ApJ, 738, 143
Ressler, J. J., Burke, J. T., Escher, J. E., et al. 2011, PhRvC, 83, 054610
Seeger, P., Fowler, W., & Clayton, D. 1965, ApJS, 11, 121
Sonnabend, K., Mohr, P., Zilges, A., et al. 2003, PhRvC, 68, 048802
Straniero, O., Chieffi, A., Limongi, M., et al. 1997, ApJ, 478, 332
Tagliente, G., Fujii, K., Milazzo, P. M., et al. 2008a, PhRvC, 77, 035802
Tagliente, G., Milazzo, P. M., Fujii, K., et al. 2008b, PhRvC, 78, 045804
Tagliente, G., Milazzo, P. M., Fujii, K., et al. 2010, PhRvC, 81, 055801
Tagliente, G., Milazzo, P. M., Fujii, K., et al. 2011a, PhRvC, 84, 015801
Tagliente, G., Milazzo, P. M., Fujii, K., et al. 2011b, PhRvC, 84, 055802
Tagliente, G., Milazzo, P. M., Fujii, K., et al. 2013, PhRvC, 87, 014622
Toukan, K. A., & Käppeler, F. 1990, ApJ, 348, 357
Travaglio, C., Gallino, R., Arnone, E., et al. 2004, ApJ, 601, 864
Utsunomiya, H., Goriely, S., Akimune, H., et al. 2010, PhRvC, 81, 035801
van Raai, M. A., Lugaro, M., Karakas, A. I., García-Hernández, D. A., & Yong, D. 2012, A&A, 540, 44
Van Winckel, H. 2003, ARA&A, 41, 391
Wallerstein, G., et al. 1997, RvMP, 69, 995
Weisskopf, V. F., & Ewing, D. H. 1940, PhRv, 57, 472
Yan, S. Q., Li, Z. H., Wang, Y. B., et al. 2016, PhRvC, 94, 015804
Younes, W., & Britt, H. C. 2003a, PhRvC, 67, 024610
Younes, W., & Britt, H. C. 2003b, PhRvC, 68, 034610
Zhang, J. S. 1992, Comm. Nucl. Data Progress, 7, 14, http://www.iaea.org/inis/collection/NCLCollectionStore/_Public/24/057/24057800.pdf
Zhang, J. S. 1993, NSE, 114, 55
Zhang, J. S. 2002, NSE, 142, 207